# Biaxial Toughening in Uniaxially Stretched Films of Block Polymer-Modified Semicrystalline Poly(L-lactide)

Jonathan P. Coote, Boran Zhao, Charles J. McCutcheon, Matthew C. Larson,
Illya Lyadov, Frank S. Bates,\* and Christopher J. Ellison\*

Department of Chemical Engineering and Material Science, University of Minnesota,

Minnesota 55455, United States

E-mail: bates001@umn.edu; cellison@umn.edu

### Abstract

Semicrystalline poly(L-lactide) (PLLA) is a leading bio-sourced, compostable alternative to conventional plastics, but lacks sufficient toughness for many applications. Chain alignment via uniaxial stretching may be used to toughen PLLA, but often creates anisotropic materials which are tough in the machine direction (MD) but brittle in the transverse direction (TD). This work reports uniaxially stretched films of PLLA blended with 3 wt % poly((ethylene oxide)-b-(butylene oxide)) (PEO-PBO)/PLLA)—which exhibit as much as a five-fold increase in toughness in the TD compared to similarly stretched neat PLLA films—and elucidates the impact of PEO-PBO particles on the relationship between stretching, crystallization behavior, and resultant mechanical properties. Faster stretching rates were correlated with higher yield stress and a greater degree of crystallite alignment in PEO-PBO/PLLA blends. This trend highlights the synergistic relationship between crystallinity and chain alignment and suggests a competing mechanism of heterogeneous crystallite nucleation around PEO-PBO particles.

Importantly, PEO-PBO/PLLA exhibited a TD elongation at break of 36%, five times greater than the value of similarly stretched neat PLLA and greater even than the corresponding MD value of either material. Taken together these findings demonstrate that uniaxial stretching of PEO-PBO/PLLA blends produce biaxially tough films, with the fastest stretching conditions producing the greatest enhancement in TD toughness.

### Keywords

sustainable plastic, polylactide, block copolymers, polymer blends, chain orientation, deformation mechanism, semicrystalline

### Introduction

The accumulation of conventional, nondegradable plastic represents a major threat to both the environment and human health across the globe. In 2016, approximately 220 million metric tons of plastic waste were produced globally, of which only 14% was recycled, while approximately 41% was mismanaged, ending up in the environment where it can persist for decades to centuries. This trend is exacerbated by the prevalence of single-use plastics, especially within the packaging industry, and highlights the need for a bio-sourced, more rapidly degradable alternative to conventional plastics.

Polylactide (PLA) is currently the most commercially viable substitute for conventional single-use packaging. It is biosourced and industrially compostable with an annual global production of 676,000 tonnes in 2023. <sup>2–9</sup> PLA is primarily systhesized from either a mixture of D- and L-lactide which produces an amorphous material (PDLLA), or from predominantly L-lactide which gives semicrystalline poly(L-lactide) (PLLA). For many applications, PLLA is preferred over its amorphous counterpart as the presence of crystal domains elevates its upper service temperature, increases yield stress and Young's Modulus, and improves its barrier properties. <sup>10–13</sup> Unfortunately, PLA of both varieties exhibits rapid physical aging, resulting

in embrittlement within hours of processing and greatly limiting the scope of applications for which it is suitable. 14–19

Toughness is often imparted to polymer films through chain alignment, which is a natural consequence of common processing methods such as cast film extrusion. <sup>20</sup> Chain alignment in these cases usually occurs in the direction of extrusion, or machine direction (MD), resulting in anisotropic, uniaxially stretched films. Previous work has shown uniaxial stretching promotes shear yielding in PLA, leading to ductile behavior when tested in the MD. <sup>21–24</sup> However, uniaxial stretching diminishes the mechanical properties of PLA when tested perpendicular to the MD, referred to as the transverse direction (TD). <sup>22,25</sup> Biaxial stretching can mitigate this imbalance, <sup>26,27</sup> but the equipment required for such processing is often prohibitively costly. <sup>28</sup> A means of biaxially toughening PLA with uniaxial stretching is therefore highly desirable.

Recently, a liquid-like disordered diblock polymer of poly(ethylene oxide)-block-poly(butylene oxide) (PEO-PBO) was shown to effectively toughen both amorphous PDLLA and semicrystalline PLLA in isotropic molded films. <sup>29,30</sup> Loadings of PEO-PBO as low as 1.8 wt% produce a morphology characterized by well-disperse macrophase separated PEO-PBO particles several hundreds of nanometers in diameter and toughened both PDLLA and PLLA through a uniform crazing mechanism, with up to a 20-fold increase in toughness at the cost of a very modest reduction in yield stress (less than 10 %) and no reduction in Young's Modulus. Significantly, this same additive was shown to provide biaxial toughening in uniaxially stretched films of amorphous PDLLA, with toughness imparted in the MD through chain alignment and in the TD through the same uniform crazing mechanism exhibited in unstretched films of PEO-PBO/PDLLA blends. <sup>31</sup>

The efficacy of PEO-PBO as a biaxial toughening agent in uniaxially stretched films of semicrystalline PLLA, however, has not yet been investigated. The presence of crystalline domains adds a great deal of complexity to the system, including how PEO-PBO impacts the degree of crystallinity, crystallization kinetics, and crystallite orientation in stretched

films, and how those variables in turn impact the mechanical performance of the films in the MD and TD. Herein, we probe these questions and investigate uniaxially stretched PEO-PBO/PLLA blend films. First, films of both neat PLLA and PEO-PBO/PLLA blends were stretched to either 200 % or 400 % of their original length at stretching rates ranging between 2 and 100 %-s<sup>-1</sup>. Second, the impact of stretching conditions on the degree of crystallinity and crystallization kinetics in both systems was investigated using differential scanning calorimetry (DSC), while crystallite structure and orientation was investigated through wide-angle X-ray scattering (WAXS). Finally, the mechanical properties in the MD and TD were investigated by room temperature tensile testing, with insight into the mechanism of deformation gleaned by visual inspection during testing.

### **Experimental Section**

Materials. Semicrystalline PLLA was purchased from NatureWorks (Ingeo 4032D). Number-average molecular weight and dispersity were determined to be  $M_n = 78 \text{ kg/mol}$  and D = 1.48, respectively, by size exclusion chromatography-multiangle light scattering (SEC-MALS) with tetrahydrofuran (THF) mobile phase and dn/dnc = 0.047 mL/g, calculated assuming 100% mass recovery. PEO-PBO diblock copolymer was purchase from Olin Corporation (trade name Fortegra 100). Number-average molecular weight was determined to be  $M_n = 7.4 \text{ kg/mol}$  by matrix-assisted laser desorption/ionization (MALDI). Dispersity was determined to be D = 1.04 by SEC-MALS with THF mobile phase. Volume fraction of PEO was determined to be 0.35 by <sup>1</sup>H NMR assuming the densities of PEO and PBO to be 1.07 and 0.92 g/mol, respectively. <sup>32</sup> Both polymers were dried under vacuum at 45 °C for 48 h before processing at elevated temperatures, but otherwise used as received.

**Blend Preparation.** A blend of 3 wt % PEO-PBO in PLLA was prepared by a previously reported masterbatch-dilution method. First, a masterbatch blend of approximately 10 wt % PEO-PBO was prepare by melt-blending PEO-PBO and PLLA in a twin screw extruder

(PRISM, 16 mm screw diameter with L/D=24:1) at 60 rpm with operating temperatures of 140, 160, 180, and 200 °C from hopper to die. The extrudate was cooled in a room temperature water bath, machine pelletized, and dried under vacuum at 40 °C for 48 h. The master-batch pellets were then dry mixed with a predetermined mass of neat PLLA pellets, then melt-blended using the same procedure to produce 3 wt% PEO-PBO/PLLA blend. Final composition was determined by <sup>1</sup>H nuclear magnetic resonance (NMR) spectroscopy. Neat PLLA pellets were melt-processed twice in the same way as the blend in order to mimic the masterbatch-dilution process.

Compression Molding. Isotropic films of neat PLLA and 3 wt% PEO-PBO/PLLA with a thickness of 500  $\mu$ m were formed by compression molding pellets between two Teflon sheets in a 180 °C Carver hydraulic press for 5 min then rapidly quenched to room temperature by compression in a second water-cooled hydraulic press within 30 s, resulting in amorphous materials in both cases. The films were then cut into 9 x 9 cm squares. A 1 cm grid was drawn with a permanent marker as a visual aid in assessing stretching uniformity.

Film Stretching. Isotropic PLLA and PEO-PBO/PLLA films were stretched uniaxially at the University of Akron's National Polymer Innovation Center using a laboratory stretching machine (KARO IV). The square films were secured with five clamps on all four sides, heated to 70 °C, and stretched at at 2, 5, 10, or 100 %-s<sup>-1</sup> to the desired stretching ratio ( $\lambda$ ) defined as

$$\lambda = \frac{L}{L_0} \tag{1}$$

where L is the length of the film after stretching and  $L_0$  is the initial length of the isotropic square sheet. The stretching force and  $\lambda$  were recorded simultaneously during stretching. Film thickness was allowed to decrease freely during stretching. Film width was held constant to allow for clearer understanding of the impact of stretching in a single dimension on the

film's properties as well as to better imitate industrial stretching processes, in which a film's width is often precisely controlled in a stenter. Once the target  $\lambda$  was reached, films were cooled to room temperature with air within 1 min.

Thermal Characterization. The thermal properties of the stretched films were determined by differential scanning calorimetry (DSC) using a Mettler Toledo DSC 1 under nitrogen. In a typical experiment, approximately 5 mg of the sample was sealed in an aluminum pan with a pinhole in the lid and heated at 10 °C/min from room temperature to 210 °C. The glass transition temperature  $(T_g)$ , melting temperature  $(T_m)$ , cold crystallization temperature  $(T_{cc})$ , enthalpy of melting  $(H_m)$ , and enthalpy of cold crystallization  $(H_c)$  were all determined from this "first heating" cycle. For the purposes of this study,  $T_m$  was defined as the onset temperature of the melting endotherm. Degree of crystallinity  $(X_c)$  was calculated by subtracting  $H_c$  from  $H_m$  and dividing the result by the enthalpy of melting for 100% crystalline PLLA, taken here to be 93.7 J/g. <sup>33</sup>

Wide-angle X-ray Scattering. Wide-angle X-ray scattering (WAXS) experiments were conducted using a Ganesha 300 XL SAXS system (SAXSLAB) with an X-ray wavelength of  $\lambda = 1.54$  Å. Films were mounted such that the direction of stretching (MD) was oriented vertically. One-dimensional (1D) traces of intensity (I) versus scattering vector (q) were obtained by integration of the two-dimensional (2D) patterns over 90° of azimuthal angle ( $\phi$ ). For 1D traces of I versus  $\phi$ , the angle of maximum intensity of the Bragg peak at q = 1.19 Å<sup>-1</sup> was defined as 90°.

Tensile Testing. Specimens for tensile experiments were prepared using a Dumbbell Co., Ltd. DSL200 equipped with an SDMK-1000 dumbbell cutter. Tests were performed at room temperature using an Instron 5966 universal tester at 1 mm/min according ASTM D1708. Reported mechanical properties were averaged over two or three separate specimens tested after aging at ambient conditions for 4 to 6 days. The number of specimens per film was

limited by the short time window available in which to test due to concerns over sample aging and by the large number of films that required testing within that window.

### Results and Discussion

Films roughly 500  $\mu$ m in thickness were compression molded from neat PLLA and a 3 wt% PEO-PBO/PLLA blend then rapidly quenched to room temperature, resulting in isotropic, amorphous films. These films were uniaxially stretched at 70 °C at varied stretching rates to  $\lambda = 2$  or  $\lambda = 4$ . The temperature was chosen such that stretching was performed above the glass transition temperature  $T_g$  but below the cold crystallization temperature  $T_{cc}$  for both neat and blend compression-molded films. As a result, crystallization at the chosen temperature occurs primarily due to stretching, with little-to-no contribution of cold crystallization. The resulting films were given names of the form  $(N/B)\lambda$ -X, where N stands for neat PLLA and B stands for PEO-PBO/PLLA blend,  $\lambda = 2$  or 4, and X stands for the stretching rate (2, 5, 10, or 100 %-s<sup>-1</sup>). For example, N4-5 is a film of neat PLLA stretched to  $\lambda = 4$  at a rate of 5 %-s<sup>-1</sup>, while B2-100 is a film of PEO-PBO/PLLA blend stretched to  $\lambda = 2$  at 100 %-s<sup>-1</sup>.

Table 1: Summary of thermal properties of uniaxially stretched films of neat PLLA and PLLA/PEO-PBO blends. All values determined from the first DSC heating scan at 10  $^{\circ}$ C/min.

Sample	$T_g$ (°C)	$T_{cc}$ (°C)	$\Delta H_c \; ({ m J/g})$	$T_m$ (°C)	$\Delta H_m  ({ m J/g})$	$X_c$ (%)
N2-100	62	86	26	160	35	10
N4-2	63	81	3	161	40	40
N4-5	64	79	4	156	41	39
N4-10	63	78	6	160	41	38
N4-100	65	77	8	157	40	35
B2-100	55	83	18	159	33	16
B4-2	53	_	_	158	40	43
B4-5	51	_	_	157	42	44
B4-10	52	_	_	160	41	43
B4-100	55	_	_	159	43	46

The thermal properties of the stretched films were characterized by DSC and are summarized in Table 1. A few trends are immediately clear and are summarized in Figure 1. First,

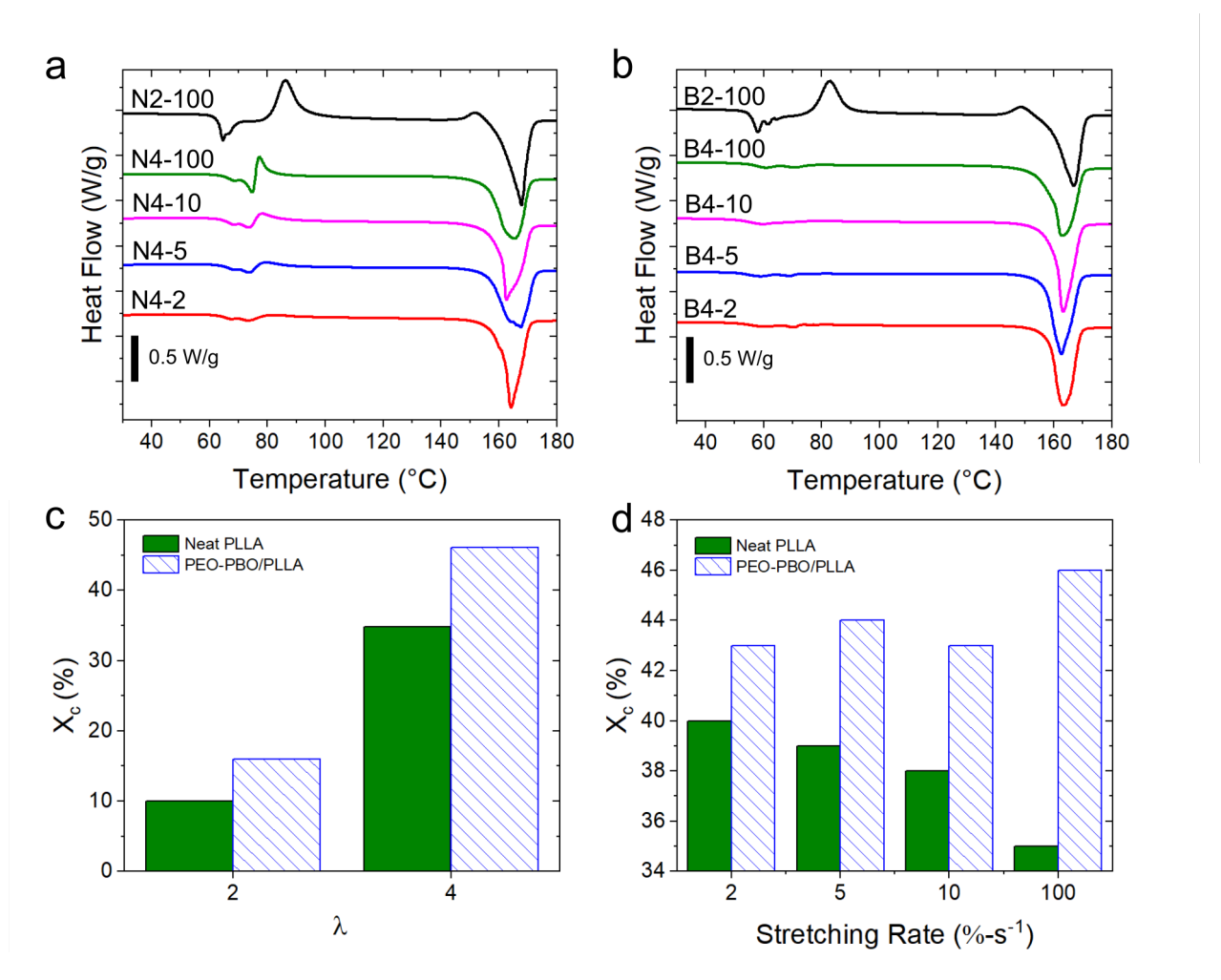


Figure 1: First heating DSC traces of (a) neat PLLA and (b) PEO-PBO/PLLA films at varied  $\lambda$  and stretching rate.  $X_C$  calculated from DSC of both neat PLLA and PEO-PBO/PLLA films is summarized as a function of (c)  $\lambda$  at a constant stretching rate of 100 %-s<sup>-1</sup> and as a function of (d) stretching rate at constant  $\lambda = 4$ .

in both neat PLLA and PEO-PBO/PLLA blend films, the degree of crystallinity  $X_c$  is quite low when  $\lambda=2$  ( $X_c=10$  % for N2-100 and 16 % for B2-100) and increases significantly when  $\lambda = 4$ , suggesting that most crystallization associated with stretching occurs at higher stretching ratios, where chains are more highly aligned in the stretching direction. Second,  $X_c$  is slightly higher and  $T_g$  is significantly lower in the PEO-PBO/PLLA blend films than in neat PLLA films, regardless of stretching ratio. This is consistent with prior results in isotropic, unstretched PEO-PBO/PLLA blend films, wherein  $X_c$  was elevated in blend films over neat PLLA by faster nucleation of crystals around the PEO-PBO particles and by the partial miscibility of PEO-PBO in the PLLA matrix, which depresses  $T_g$  by roughly 10 °C.<sup>30</sup> Finally, at  $\lambda = 4$ , the blend films exhibit the opposite relationship between stretching rate and  $X_c$  as neat PLLA films. In the neat films,  $X_c$  decreases as stretching rate increases, whereas in blend films  $X_c$  increases as stretching rate increases. This difference can also be attributed to the partial miscibility of PEO-PBO in the PLLA matrix. PLLA is known to exhibit relatively slow crystallization kinetics. 34,35 In neat PLLA, faster stretching rates likely afford less time for the PLLA chains to reorient and crystallize before the stretching is halted and the film is cooled below  $T_g$ , resulting in lower overall  $X_C$  than is obtained with slow stretching. In the PEO-PBO/PLLA blend films, by contrast, partially miscible PEO-PBO increases the mobility of the PLLA chains and therefore decreases the timescales of chain reorientation and crystallization relative to that of film stretching, such that the bulk of crystallization is complete before stretching is finished and the film is cooled, regardless of stretching rate. This interpretation is further supported by the observation that while the  $\Delta H_c$  in the neat PLLA films increases with increasing stretching rate, no cold crystallization is observed in the PEO-PBO/PLLA blend films.

Wide-angle X-ray scattering (WAXS) experiments were performed in order to gain a better understanding of the impact of  $\lambda$  and stretching rate on the formation and alignment of crystals in neat PLLA and PEO-PBO/PLLA blend films (2D scattering data for all films are provided in Figure S1 in the Supporting Information). For  $\lambda = 2$ , little-to-

no crystallite scattering is observed for either neat PLLA or PEO-PBO/PLLA blend films stretched at 100 %-s<sup>-1</sup>. This is consistent with the thermal characterization of  $X_C$ —while a small degree of crystallinity is measureable in DSC for these films, the associated WAXS scattering is sufficiently weak so as to be obscured by the amorphous halo. When  $\lambda = 4$ , significant scattering associated with PLLA crystallites is observed for both neat PLLA and PEO-PBO/PLLA blend films (Figure S2), again in agreement with thermal characterization of  $X_C$ . In addition, while the intensity of the (200)/(110) peak at q=1.19 Å $^{-1}$  decreases with stretching rate in neat PLLA films, intensity increases with stretching rate in PEO-PBO/PLLA blend films. This suggests that  $X_C$  also increases with increasing stretching rate, consistent with the trends observed in  $X_c$  obtained from DSC. Furthermore, in neat PLLA films, the (200)/(110) peak broadens as stretching rate increases, and no broadening is observed in PEO-PBO/PLLA blend films (full-width at half-max obtained from Gaussian fit to scattering peaks shown in Figure S3). As the Scherrer equation gives an inverse relationship between peak breadth and mean crystal size, it can be inferred that faster stretching in neat PLLA films results in smaller crystals, while crystal size in PEO-PBO/PLLA blends is roughly unchanged by stretching rate.<sup>36</sup>

The effect of stretching rate on crystallite alignment is noticeably different between the neat PLLA and PEO-PBO/PLLA films. While the Bragg peaks exhibited by the neat PLLA films broaden in q with stretching rate, their breadth remains constant along the azimuthal angle  $\phi$ , suggesting that, while crystal sizes decreases with stretching rate, there is no change in overall degree of crystallite alignment (Figure 2a). Inversely, the peaks exhibited by PEO-PBO/PLLA are significantly broader in  $\phi$  than those of neat PLLA at slower stretching rates, but sharpen as stretching increases (Figure 2b), indicating that while crystallite size remains constant with stretching rate in PEO-PBO/PLLA films, faster stretching produces more highly aligned crystallites. Quantification of the degree of crystallite orientation from the WAXS data by means of the Hermans orientation function supports this trend (Figure S4).  $^{37-39}$  Since it has been previously argued that PEO-PBO particles act as nucleation

agents for PLLA for crystallization, <sup>30</sup> this trend may be explained by a competition between heterogeneous nucleation of crystallites around PEO-PBO particles on the one hand and homogeneous nucleation throughout the PLLA matrix due to chain alignment on the other, as illustrated in Figure 3. It has been shown when PLLA films are stretched at temperatures above  $T_g$ , crystallite nucleation and growth due to chain alignment occur primarily above a critical stretching ratio  $\lambda_C$ . <sup>40,41</sup> When a heterogeneous nucleation agent such as talc is employed, enhanced crystallization rates around the particles are observed below  $\lambda_C$ , opening up a competing nucleation mechanism. <sup>42</sup> In the case of PEO-PBO/PLLA films, which are slowly stretched spend a relatively long time at  $\lambda < \lambda_C$ , where heterogeneous nucleation localized around the PEO-PBO particles dominates. In constrast, when films are rapidly stretched to  $\lambda > \lambda_C$  (for reference, the entire stretching process lasts just 3 s at 100%-s<sup>-1</sup>), chain alignment-induced nucleation in the PLLA matrix would compete more significantly with heterogeneous nucleation around the PEO-PBO particles. Because heterogeneous nucleation dominates at low values of  $\lambda$  where chains are less aligned, it follows that crystallites in slowly-stretched films would be more isotropic than those in fast-stretched films.

This interpretation is further supported by examining the force of stretching as a function of  $\lambda$ , collected during film stretching at 70 °C (Figure S5). Both neat PLLA and PEO-PBO/PLLA films exhibit a broad yielding transition followed by a region of strain hardening around  $\lambda = 3$ , likely due to the growth of crystals and consistent with the large increase in  $X_c$  between  $\lambda = 2$  and  $\lambda = 4$ . This suggests that  $\lambda_C$  for this system may be in the vicinity of  $\lambda = 3$ . A significant difference can be seen between the strain hardening behavior of neat PLLA and PEO-PBO/PLLA blend films. Both the onset of strain hardening and the final stretching force reached at  $\lambda = 4$  in neat PLLA films is approximately the same regardless of stretching rate. In PEO-PBO/PLLA blend films, the onset of strain hardening shifts monotonically to higher  $\lambda$  as stretching rate increases, and the final stretching force is inversely correlated to stretching rate. The slope of strain hardening remains roughly constant with stretching rate. This behavior is consistent with competing nucleation mechanisms occurring at different  $\lambda$ .

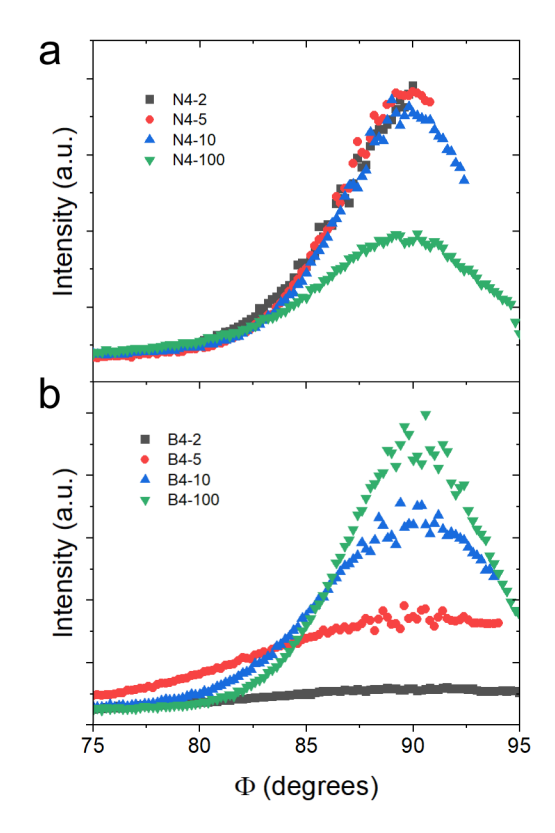


Figure 2: Intensity vs azimuthal angle  $\phi$  in 1D WAXS for (a) neat PLLA and (b) PEO-PBO/PLLA films stretched to  $\lambda=4$  at varied stretching rate. Data within each panel are on the same relative intensity scale.

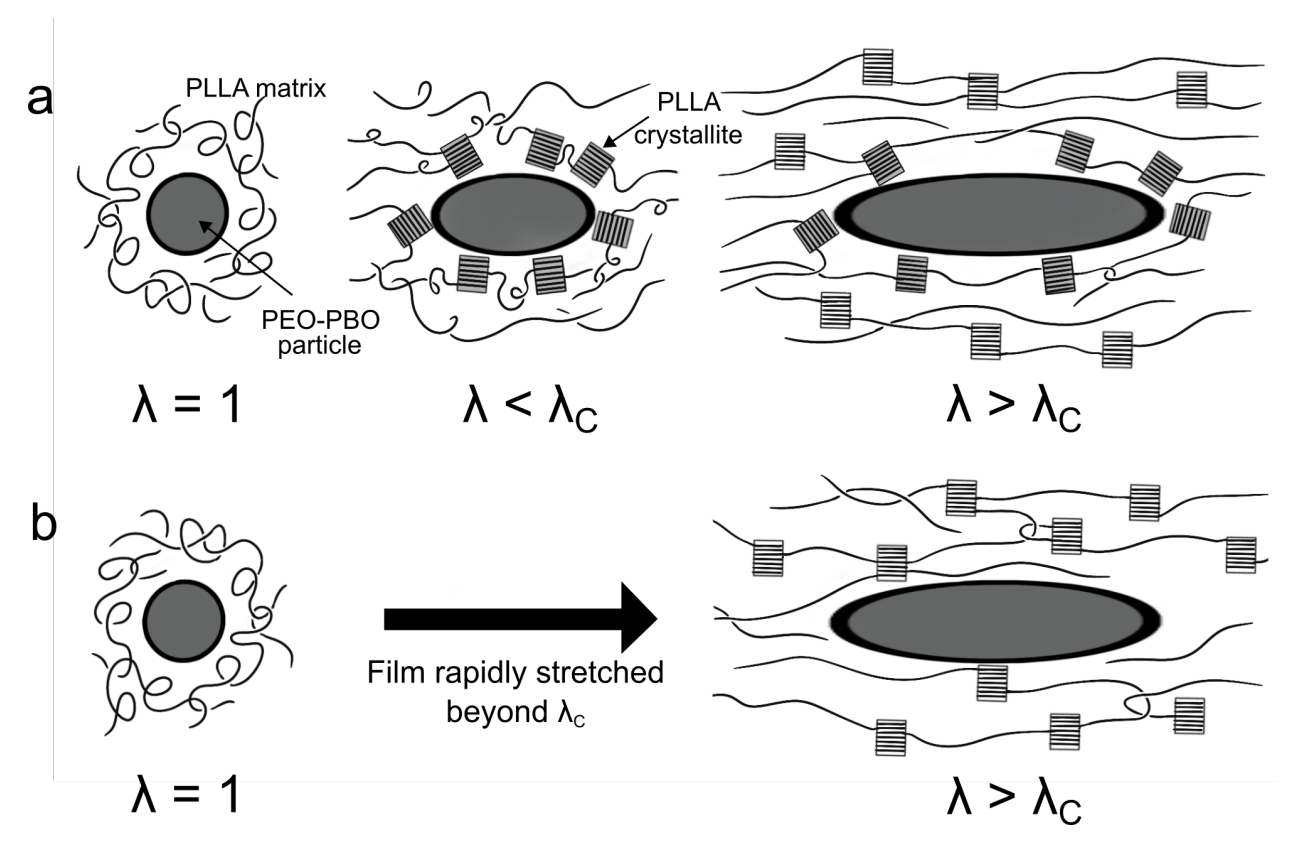


Figure 3: An illustration of the proposed impact of stretching rate on the crystallite alignment in (a) slow-stretched and (b) fast-stretched PEO-PBO/PLLA blend films. The sizes of PLLA chains and crystallites are exaggerated relative to the PEO-PBO particle for the sake of clarity.

At slow stretching rates, heterogeneous nucleation around PEO-PBO particles results in higher  $X_C$  at lower  $\lambda$ . This leads to the onset of strain hardening at lower  $\lambda$  and therefore to strain hardening over a wide range of  $\lambda$ , ultimately resulting in a higher final stretching force at  $\lambda = 4$ .

Table 2: Summary of the mechanical properties of neat PLLA and PEO-PBO/PLLA blend films. Sample names ending in "M" indicate samples tested in the MD, while names ending in "T" indicate samples tested in the TD.

Sample	$X_c$ (%)	$\sigma_Y$ (MPa)	E (GPa)	$\varepsilon_B$ (%)	Toughness $(MJ/m^3)$
N2-100M	10	$94 \pm 3$	$3.4 \pm 0.2$	$94 \pm 3$	$54 \pm 2$
N4-2M	40	$107 \pm 4$	$5.1 \pm 0.1$	$24 \pm 1$	$25\pm2$
N4-5M	39	$103 \pm 2$	$5.2 \pm 0.1$	$27 \pm 4$	$28 \pm 4$
N4-10M	38	$106 \pm 3$	$5.2 \pm 0.1$	$24 \pm 2$	$24 \pm 3$
N4-100M	35	$101 \pm 2$	$5.4 \pm 0.1$	$28 \pm 2$	$31 \pm 4$
B2-100M	16	$63 \pm 4$	$3.4 \pm 0.2$	$80 \pm 19$	$44 \pm 9$
B4-2M	43	$76 \pm 3$	$4.5 \pm 0.2$	$32 \pm 9$	$25 \pm 7$
B4-5M	44	$77 \pm 2$	$4.6 \pm 0.2$	$32 \pm 9$	$26 \pm 8$
B4-10M	43	$88 \pm 2$	$5.1 \pm 0.1$	$30 \pm 1$	$28 \pm 1$
B4-100M	46	$95 \pm 2$	$5.3 \pm 0.1$	$26 \pm 3$	$25 \pm 4$
N2-100T	10	$64 \pm 1$	$3.0 \pm 0.1$	$6 \pm 3$	$3\pm 2$
N4-2T	40	$48 \pm 5$	$3.2 \pm 0.2$	$7 \pm 5$	$3\pm 2$
N4-5T	39	$55 \pm 1$	$2.6 \pm 0.1$	$5 \pm 1$	$2 \pm 1$
N4-10T	38	$49 \pm 7$	$2.3 \pm 0.2$	$6 \pm 1$	$2 \pm 1$
N4-100T	35	$57 \pm 2$	$2.7 \pm 0.1$	$7 \pm 1$	$3\pm1$
B2-100T	16	$47 \pm 2$	$3.1 \pm 0.1$	$33 \pm 10$	$12 \pm 3$
B4-2T	43	$48 \pm 2$	$2.5 \pm 0.1$	$12 \pm 8$	$5\pm3$
B4-5T	44	$44 \pm 1$	$2.6 \pm 0.1$	$26 \pm 10$	$9 \pm 4$
B4-10T	43	$47 \pm 1$	$2.7 \pm 0.1$	$28 \pm 1$	$11 \pm 1$
B4-100T	46	$41 \pm 1$	$2.6 \pm 0.1$	$36 \pm 11$	$13 \pm 4$

Room temperature tensile experiments, summarized in Table 2, were performed in order to probe the impact of stretching and the resulting alignment of chains and crystallites on the mechanical properties of PLLA and PEO-PBO/PLLA blends. An "M" or a "T" is appended to the end of the sample name to indicate that the sample was tested in the MD or the TD, respectively. In the MD, neat PLLA films stretched to  $\lambda = 2$  exhibited ductile behavior, with a roughly 10-fold increase in elongation at break  $(\varepsilon_B)$  over unstretched PLLA (Figure 4a). Further stretching, however, decreases the ductility of the films while significantly increasing

yield stress ( $\sigma_Y$ ), Young's Modulus (E), and the rate of strain hardening, consistent with both the higher  $X_C$  and higher  $\lambda$ . <sup>30,31</sup> The impact of  $\lambda$  on the mechanical properties of PEO-PBO/PLLA films in the MD was nearly identical to its impact on neat PLLA, though  $\sigma_Y$  was slightly lower in PEO-PBO/PLLA blends than in neat PLLA due to the partial miscibility of PEO-PBO in PLLA, consistent with behavior reported previously in unstretched PEO-PBO/PLLA films. <sup>31</sup>

It is important to point out here the synergistic influence of  $X_C$  and  $\lambda$  in the MD. To illustrate this point, Figure S6 summarizes previously reported  $\sigma_Y$  of unstretched amorphous PDLLA, <sup>29</sup> unstretched PLLA ( $X_C = 30\%$ ), <sup>30</sup> PDLLA stretched to  $\lambda = 4$ , <sup>31</sup> and sample N4-5, all normalized by  $\sigma_Y$  of unstretched PDLLA (all tested in the MD, where applicable). The addition of crystallinity in PLLA unstretched films produces a roughly 25% increase in  $\sigma_Y$  over unstretched PDLLA. Likewise, stretching PDLLA to  $\lambda = 4$  produces a roughly 25% increase in  $\sigma_Y$ . The combination of crystallinity and uniaxial stretching, however, increases  $\sigma_Y$  by more than 100%, illustrating the out-sized impact of crystallite alignment on mechanical properties in these films.

In the TD, neat PLLA films are brittle regardless of  $\lambda$ , with dramatic reduction in E,  $\sigma_Y$ ,  $\varepsilon_B$ , and toughness compared to the MD due to chain alignment perpendicular to the testing direction. PEO-PBO/PLLA films, however, exhibit a significant increase in ductility in the TD over neat PLLA (Figure 4b). Elongation at break increases from 7% in the PLLA films to as much as 36% in B4-100T, greater even than the corresponding MD value in B4-100M. This is likely due, counter-intuitively, to the lack of chain alignment in the direction of testing, which in contrast to the MD does not result in strain hardening and allows for almost entirely ductile behavior in PEO-PBO/PLLA blends via uniform crazing. <sup>31</sup> The result is an increase in toughness by as much as a factor of five with little apparent dependence on  $\lambda$ .

The impact of stretching rate on the mechanical performance of PLLA and PEO-PBO/PLLA films in the MD and TD was also investigated. Representative tensile date for PEO-PBO/PLLA blends in the MD and TD are shown in Figure 4c, and trends in E,

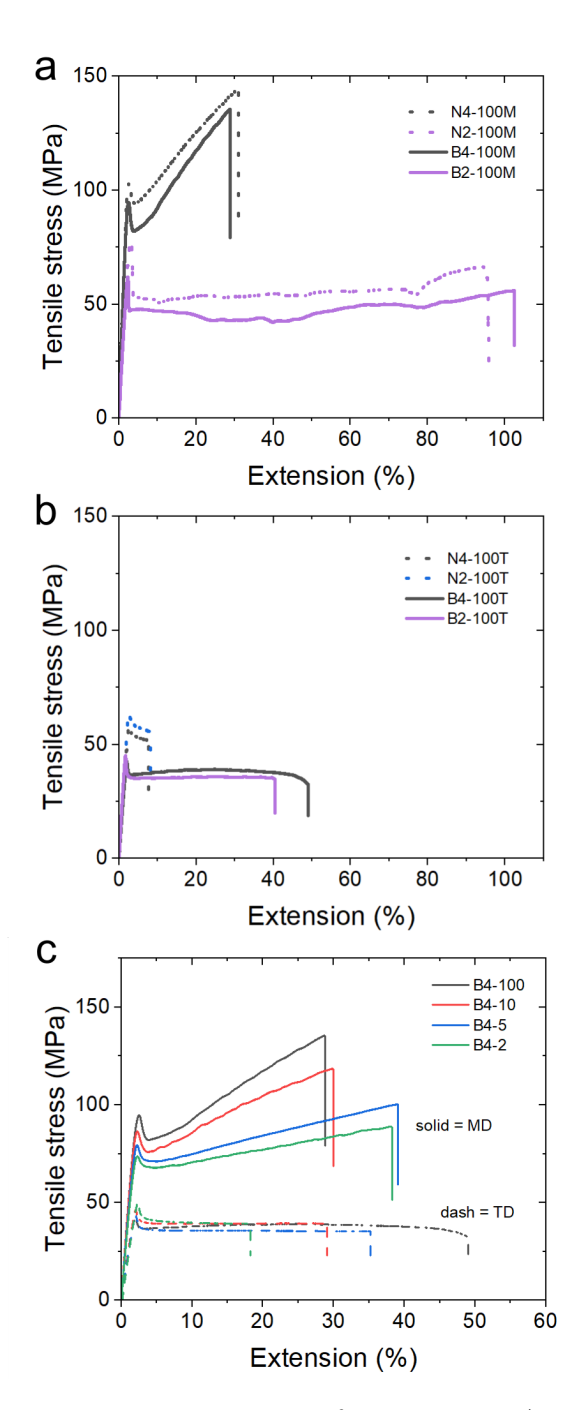


Figure 4: Representative stress-strain curves for neat PLLA and PEO-PBO/PLLA films tested in (a) the MD or (b) the TD and stretched to varied  $\lambda$  at 100 %-s<sup>-1</sup>, as well as (c) PEO-PBO/PLLA films stretched to  $\lambda=4$  at varied stretching rates.

 $\sigma_Y$ ,  $\varepsilon_B$ , and tensile toughness in both neat PLLA and PEO-PBO/PLLA films are summarized for the MD and TD in Figures 5 and 6, respectively. In both the MD and TD, stretching rate appears to play little role in the mechanical performance of neat PLLA. In contrast, there is a strong influence of stretching rate on the mechanical properties of PEO-PBO/PLLA films in both the MD and TD. As stretching rate increases, PEO-PBO/PLLA films tested in the MD exhibit significant increase in  $\sigma_Y$  (from 77 MPa in B4-2M to 95 MPa in B4-100M) and decrease in  $\varepsilon_B$  (from 32 % in B4-2 to 26 % in B4-100), as well as a slight increase in E (4.5 GPa in B4-2 to 5.3 GPa in B4-100), with B4-100M exhibiting very similar behavior to neat PLLA films tested in the MD (Figure 5). Moreover, faster stretching is correlated with more rapid strain hardening when tested in the MD (Figure 4c). This trend is consistent with increasing degree of crystallite alignment with faster stretching observed in WAXS in PEO-PBO/PLLA but absent in neat PLLA films. This is particularly interesting as it suggests that crystal alignment has a far greater impact on mechanical properties in these films than does crystal size, which analysis of WAXS peak breadth (Figure S3) suggests varies with stretching rate in neat PLLA but not in PEO-PBO/PLLA blends.

In the TD,  $\varepsilon_B$  and toughness in PEO-PBO/PLLA films increase significantly as a function of stretching rate, with toughness increasing from 5 MJ/m<sup>3</sup> in B4-2 to 13 MJ/m<sup>3</sup> in B4-100 (Figure 6). This trend may be explained by a difference in the degree to which crystallites are localized around PEO-PBO particles at different stretching rates and the way in which that localization interferes with craze growth, depicted schematically in Figure 7. As previously discussed, slowly-stretched films spend more time at  $\lambda < \lambda_C$ , where heterogeneous nucleation of crystallites around the PEO-PBO particles dominates, while at faster stretching rates chain alignment-induced homogeneous nucleation competes more strongly. This also means that crystallites are localized near the PEO-PBO particles to a greater degree in slow-stretched films than in fast-stretched ones. The crowding of crystallites around the PEO-PBO particles, therefore, may limit the size to which a craze can grow before it is hindered by a crystallite. As the mechanism of toughening imparted by PEO-PBO is de-

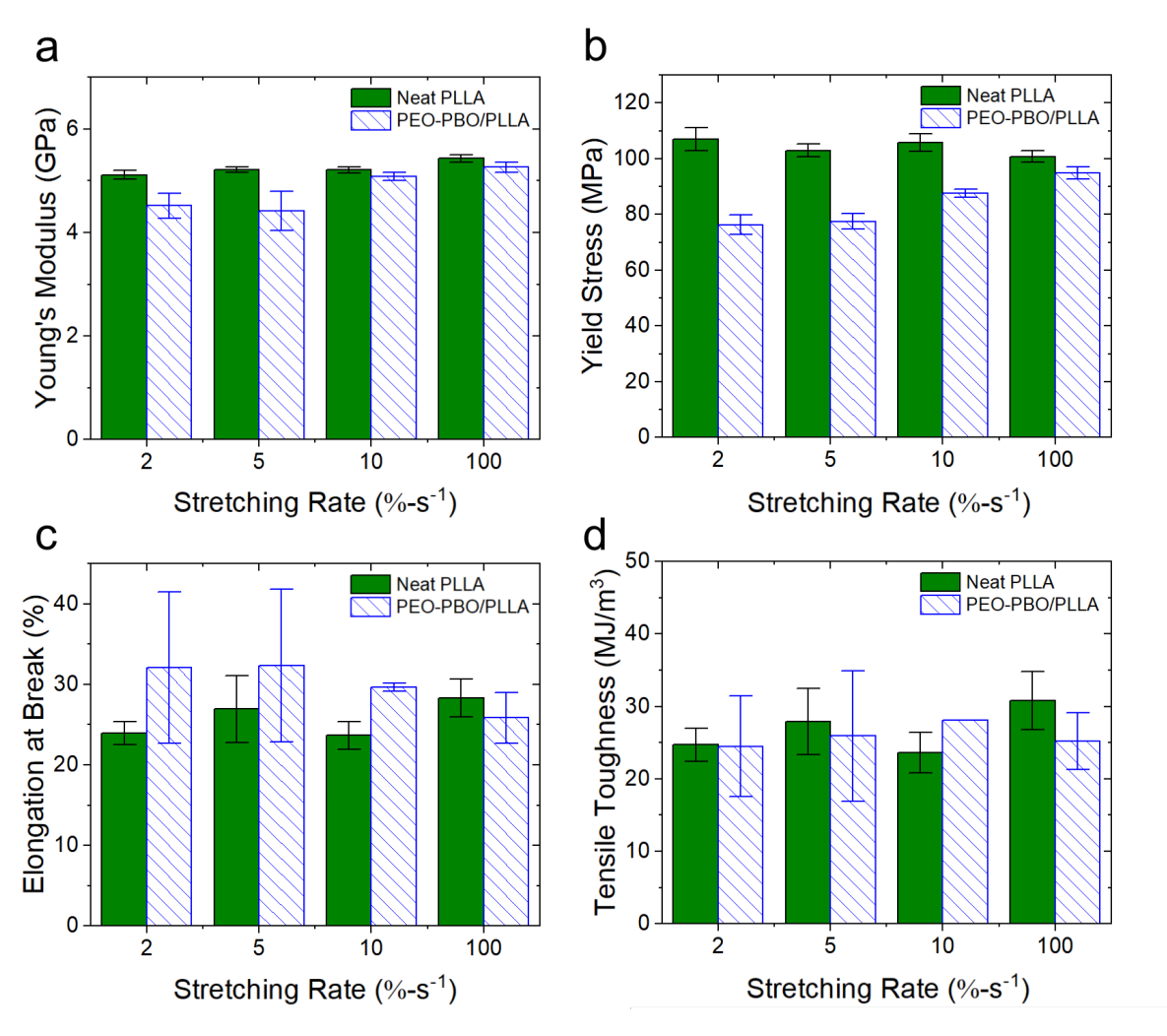


Figure 5: Summary of (a) Young's Modulus, (b) yield stress, (c) elongation at break, and (d) tensile toughness in neat PLLA and PEO-PBO/PLLA films tested in the MD. All films were stretched to  $\lambda=4$ .

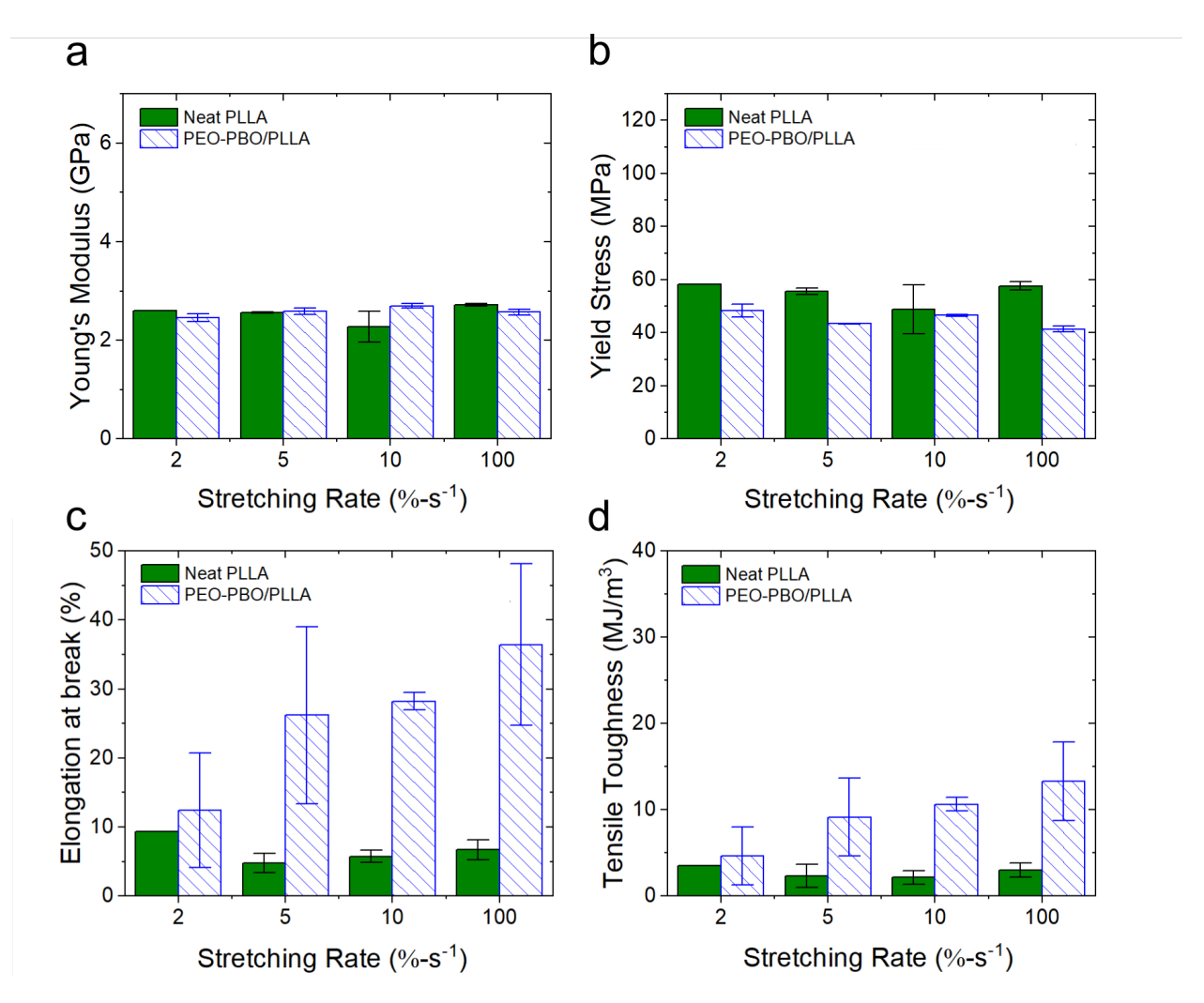


Figure 6: Summary of (a) Young's Modulus, (b) yield stress, (c) elongation at break, and (d) tensile toughness in neat PLLA and PEO-PBO/PLLA films tested in the TD. All films were stretched to  $\lambda=4$ .

pendent on uniform craze initiation by cavitation of compliant PEO-PBO particles and the enhancement of craze growth, the restriction of craze growth by crystallite crowding would necessarily result in a loss of toughness in the TD.

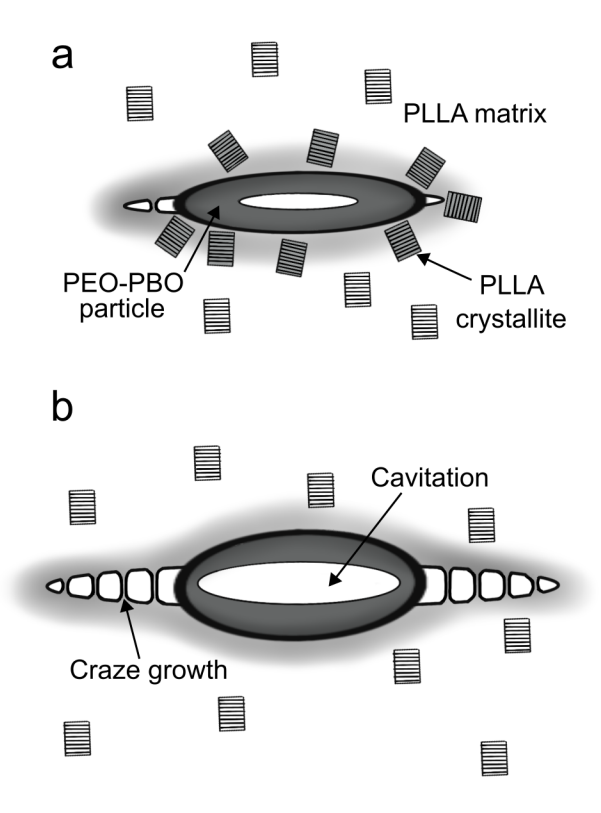


Figure 7: An illustration of the proposed influence of crystallite crowding on craze growth in (a) slow-stretched versus (b) fast-stretched PEO-PBO/PLLA films. The size of PLLA crystallites is exaggerated relative to the PEO-PBO particle for the sake of clarity.

In order to elucidate the impact of stretching conditions on the mechanism of deformation in neat PLLA and PEO-PBO/PLLA films, photographs were taken of tensile bars at various stages of deformation during tensile experiments. Representative sets of photographs are provided in Figure 8. All tensile bars were initially transparent, consistent with the formation of PLLA nanocrystallites, known to form during melt stretching of PLLA. <sup>43</sup> These nanocrystallites are too small to scatter light in the visible spectrum, resulting in optically transparent films despite a relatively high degree of crystallinity for PLLA. For neat PLLA samples, tensile bars remained transparent upon elongation in the MD and de-

formed uniformly by thinning, indicative of uniform shear yielding. In the TD, tensile bars also remained transparent throughout the deformation process, but brittleness due to chain alignment normal to the direction of testing meant that very little deformation took place. These behaviors were observed regardless of  $\lambda$  or stretching rate.

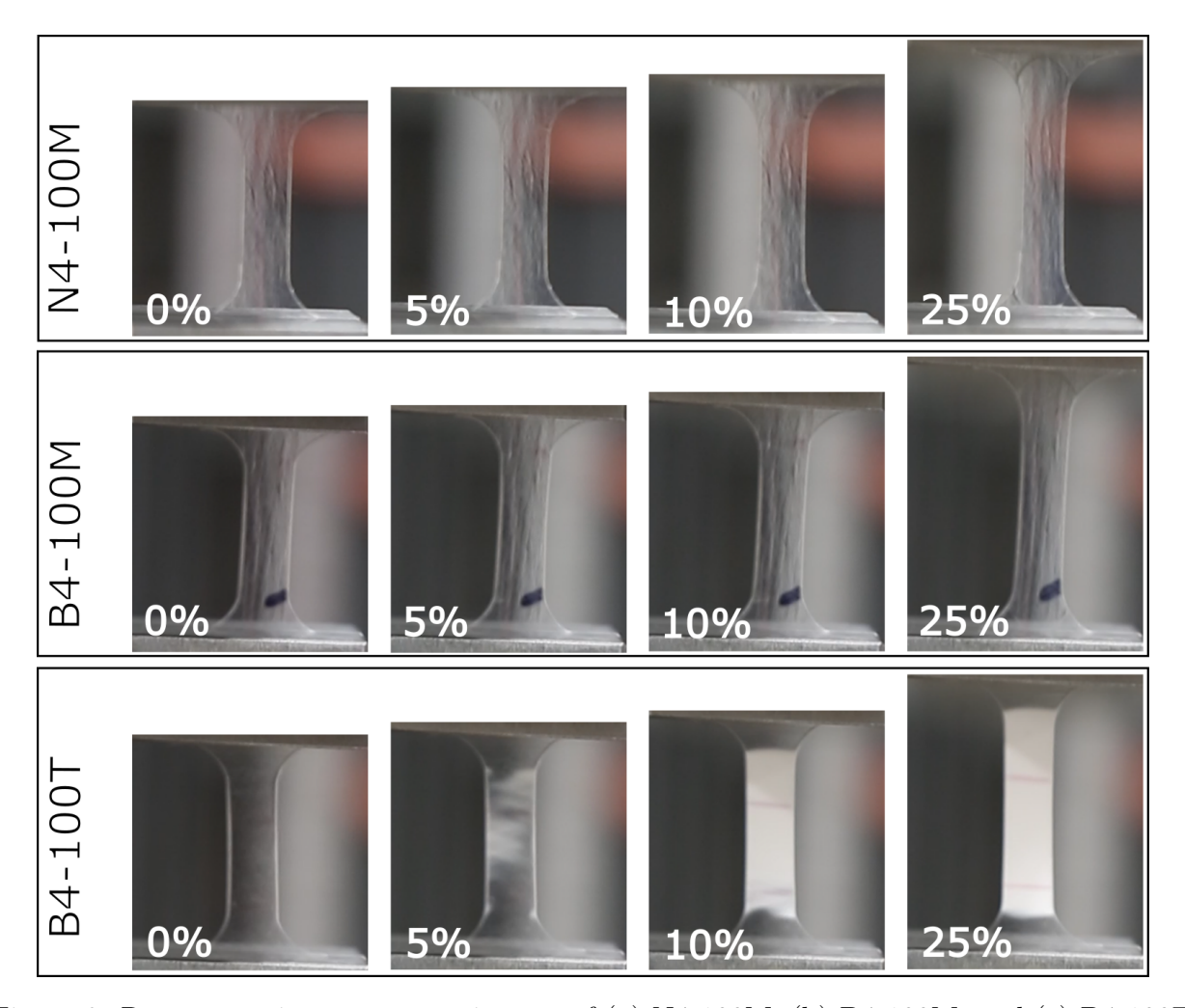


Figure 8: Representative gauge area images of (a) N4-100M, (b) B4-100M, and (c) B4-100T during deformation to varied strain percents.

Unlike in the neat PLLA films, the deformation mechanism in PEO-PBO/PLLA films exhibited a dependence on both  $\lambda$  and testing direction. In the MD, PEO-PBO/PLLA films stretched to  $\lambda=4$  deform nearly identically to neat PLLA films. This is in contrast to unstretched PEO-PBO/PLLA films which deform by uniform crazing, as previously reported. In sample B2-100M, deformation begins by local deformation followed by neck

formation at around 10% strain, and only at higher strains does the necked region begin to whiten (Figure S7). This suggests that even  $\lambda=2$  is sufficient to shift the dominant deformation mechanism from crazing to shear yielding. In sample B4-100, no whitening is observed during deformation at all, indicating a complete shift to shear yielding. In the TD, by contrast, PEO-PBO/PLLA deformation for  $\lambda=2$  or 4 is characterized by uniform whitening of the gauge region shortly after yielding, consistent with deformation by uniform crazing previously observed in isotropic PEO-PBO/PLLA blends. <sup>30</sup> In addition, this difference in deformation mechanism between yielding in the MD and crazing in the TD has previously been observed in uniaxially-stretched blends of PEO-PBO with amorphous PDLLA. In the MD, chain alignment in the drawing direction reduces the stress of shear yielding relative to craze stress, making shear yielding the dominant mechanism of deformation. <sup>31</sup> In the TD, in which chain alignment is perpendicular to the drawing direction, the inverse is true—due to lack of chain alignment and to the capacity of PEO-PBO particles to cavitate and initiate crazes, craze stress remains lower that the stress of shear yielding, and the samples deform primarily by uniform crazing. <sup>29</sup>

### Conclusions

Uniaxial stretching was found to toughen both PLLA and PEO-PBO/PLLA in the MD, but only PEO-PBO/PLLA exhibited increased toughness in the TD. Toughness in the MD was imparted in both cases by chain alignment, which promotes shear yielding. In the TD, perpendicular to chain alignment, neat PLLA is brittle while PEO-PBO/PLLA is toughened by uniform crazing promoted by the PEO-PBO particles. Stretching ratio  $\lambda$  was shown to have a significant impact on degree of crystallinity and crystallite alignment in both neat PLLA and PEO-PBO/PLLA blends, which in turn influence mechanical properties. At  $\lambda = 2$ ,  $X_C$  is low, and ductile behavior is observed in the MD, while at  $\lambda = 4$   $X_C$  is as high as 40 % in neat PLLA and 46 % in PEO-PBO/PLLA blends. Moreover, the resulting crystal-

lites are aligned in the MD, leading to significantly increased  $\sigma_Y$ , E, and strain hardening. Stretching rate did not significantly impact the crystallite alignment or mechanical properties of neat PLLA, as crystallization kinetics are slow relative to the rate of stretching. In PEO-PBO/PLLA, however, the combination of partial miscibility of PEO-PBO in PLLA and the rapid nucleating effect of the PEO-PBO particles accelerates crystallization kinetics. In particular, the competition between hetergeneous nucleation of crystallites around PEO-PBO particles and homogeneous nucleation in the PLLA matrix due to stretching results in more isotropic crystallites at slow stretching rates and more highly aligned crystallites at faster stretching rates. Crystallites highly aligned in the MD provide reinforcement to the material, increasing  $\sigma_Y$  in that direction for both neat PLLA and PEO-PBO/PLLA. Interestingly, fast stretching increases toughness in the TD more than slow stretching in PEO-PBO/PLLA blends, possibly due to the lack of crowding crystallites near the PEO-PBO particles, which are likely more prevalent in slow-stretched films due to the nucleating effect of PEO-PBO particles at low  $\lambda$ . These findings demonstrate that uniaxial stretching of PEO-PBO/PLLA produces films with biaxial enhancement in toughness, with the fastest processing conditions producing the most desirable results, increasing the competitiveness of PLLA as a sustainable alternative to conventional plastics.

## Acknowledgement

This work was supported primarily by the farm families of Minnesota and their corn check-off investment and in part by the National Science Foundation Center for Sustainable Polymers at the University of Minnesota, a Center for Chemical Innovation (CHE-1901635). Part of this work was conducted in the Characterization Facility at the University of Minnesota, which receives partial support from the NSF through the MRSEC program (DMR-2011401). Film stretching was carried out by Todd Lewis in the National Polymer Innovation Center (NPIC) at the University of Akron.

**Supporting Information:** 2D WAXS patterns for all samples; full-width at half-max (FWHM) of primary WAXS peaks (intensity vs q); Hermans orientation function values derived from WAXS ( $\phi$  vs q); representative images of B2-100 during deformation to strains between 0% and 50%.

### References

- (1) Breaking the Plastic Wave: A Comprehensive Assessment of Pathways Towards Stopping Ocean Plastic Pollution; The Pew Charitable Trusts, 2020.
- (2) Vink, E. T.; Davies, S. Life Cycle Inventory and Impact Assessment Data for 2014 Ingeo(R) Polylactide Production. *Industrial Biotechnology* **2015**, *11*, 167–180.
- (3) Miller, S. A. Sustainable polymers: Opportunities for the next decade. *ACS Macro Letters* **2013**, *2*, 550–554.
- (4) Lim, L. T.; Auras, R.; Rubino, M. Processing technologies for poly(lactic acid). *Progress in Polymer Science (Oxford)* **2008**, *33*, 820–852.
- (5) Kale, G.; Kijchavengkul, T.; Auras, R.; Rubino, M.; Selke, S. E.; Singh, S. P. Compostability of bioplastic packaging materials: An overview. *Macromolecular Bioscience* 2007, 7, 255–277.
- (6) Sardon, H.; Dove, A. P. Plastics recycling with a difference: A novel plastic with useful properties can easily be recycled again and again. *Science* **2018**, *360*, 380–381.
- (7) Albertsson, A. C.; Hakkarainen, M. Designed to degrade. Science 2017, 358, 872–873.
- (8) Jem, K. J.; Tan, B. The development and challenges of poly (lactic acid) and poly (glycolic acid). Advanced Industrial and Engineering Polymer Research 2020, 3, 60–70.

- (9) Bioplastic Market Development Update 2023; European Bioplastics, 2023.
- (10) Deng, L.; Xu, C.; Wang, X.; Wang, Z. Supertoughened Polylactide Binary Blend with High Heat Deflection Temperature Achieved by Thermal Annealing above the Glass Transition Temperature. ACS Sustainable Chemistry and Engineering 2018, 6, 480– 490.
- (11) Tábi, T.; Hajba, S.; Kovács, J. G. Effect of crystalline forms ( and ) of poly(lactic acid) on its mechanical, thermo-mechanical, heat deflection temperature and creep properties. *European Polymer Journal* **2016**, *82*, 232–243.
- (12) Hashima, K.; Nishitsuji, S.; Inoue, T. Structure-properties of super-tough PLA alloy with excellent heat resistance. *Polymer* **2010**, *51*, 3934–3939.
- (13) Ahmed, J.; Varshney, S. K. Polylactides-chemistry, properties and green packaging technology: A review. *International Journal of Food Properties* **2011**, *14*, 37–58.
- (14) Struik, L. C. Physical aging in plastics and other glassy materials. *Polymer Engineering Science* **1977**, *17*, 165–173.
- (15) Arnold, J. C. The effects of physical aging on the brittle fracture behavior of polymers.

  \*Polymer Engineering Science 1995, 35, 165–169.
- (16) Haugan, I. N.; Lee, B.; Maher, M. J.; Zografos, A.; Schibur, H. J.; Jones, S. D.; Hillmyer, M. A.; Bates, F. S. Physical Aging of Polylactide-Based Graft Block Polymers. *Macromolecules* 2019, 52, 8878–8894.
- (17) Pan, P.; Zhu, B.; Inoue, Y. Enthalpy Relaxation and Embrittlement of Poly(1-lactide) during Physical Aging. *Macromolecules* **2007**, *40*, 9664–9671.
- (18) Theryo, G. C.; Hillmyer, M. A. Deformation and Physical Aging of Rubber-Modified Polylactide Graft Copolymers. Ph.D. thesis, University of Minnesota, 2014.

- (19) Ren, J.; Urakawa, O.; Adachi, K. Dielectric and viscoelastic studies of segmental and normal mode relaxations in undiluted poly(d,l-lactic acid). *Macromolecules* 2003, 36, 210–219.
- (20) Tamdor, Z. *Principles of Polymer Processing*, 2nd ed.; John Wiley Sons, 2013; pp 705–720.
- (21) Guo, Y.; Peng, S.; Wang, Q.; Song, X.; Li, C.; Xia, L.; Wu, H.; Guo, S. Achieving High-Ductile Polylactide Sheets with Inherent Strength via a Compact and Uniform Stress Conduction Network. *Industrial and Engineering Chemistry Research* 2020, 59, 12096–12105.
- (22) Razavi, M.; Cheng, S.; Huang, D.; Zhang, S.; Wang, S. Q. Crazing and yielding in glassy polymers of high molecular weight. *Polymer* **2020**, *197*.
- (23) Razavi, M.; Wang, S. Q. Double Yielding in Deformation of Semicrystalline Polymers.

  \*Macromolecular Chemistry and Physics 2020, 221, 2000151.
- (24) Gao, X. R.; Li, Y.; Huang, H. D.; Xu, J. Z.; Xu, L.; Ji, X.; Zhong, G. J.; Li, Z. M. Extensional Stress-Induced Orientation and Crystallization can Regulate the Balance of Toughness and Stiffness of Polylactide Films: Interplay of Oriented Amorphous Chains and Crystallites. *Macromolecules* 2019, 52, 5278–5288.
- (25) Zartman, G. D.; Cheng, S.; Li, X.; Lin, F.; Becker, M. L.; Wang, S. Q. How melt-stretching affects mechanical behavior of polymer glasses. *Macromolecules* **2012**, *45*, 6719–6732.
- (26) Demeuse, M. T. In *Other polymers used for biaxial films*; DeMeuse, M. T., Ed.; Woodhead Publishing, 2011; pp 47–58.
- (27) Zhou, H.; Song, Z.; Cai, S. Toughening of poly(lactide acid) with low crystallinity through biaxial poststretching. *Journal of Polymer Science* **2020**, *58*, 3488–3495.

- (28) Lin, Y.; Chen, W.; Meng, L.; Wang, D.; Li, L. Recent advances in post-stretching processing of polymer films with: In situ synchrotron radiation X-ray scattering. *Soft Matter* **2020**, *16*, 3599–3612.
- (29) McCutcheon, C. J.; Zhao, B.; Jin, K.; Bates, F. S.; Ellison, C. J. Crazing Mechanism and Physical Aging of Poly(lactide) Toughened with Poly(ethylene oxide)-block-poly(butylene oxide) Diblock Copolymers. *Macromolecules* **2020**, *53*, 10163–10178.
- (30) McCutcheon, C. J.; Zhao, B.; Ellison, C. J.; Bates, F. S. Crazing and Toughness in Diblock Copolymer-Modified Semicrystalline Poly(l-lactide). *Macromolecules* 2021, 54, 11154–11169.
- (31) Zhao, B.; McCutcheon, C. J.; Jin, K.; Lyadov, I.; Zervoudakis, A. J.; Bates, F. S.; Ellison, C. J. Enhanced Mechanical Properties of Uniaxially Stretched Polylactide/ Poly(ethylene oxide)-b-Poly(butylene oxide) Blend Films. ACS Applied Polymer Materials 2022, 4, 8705–8714.
- (32) Wu, J.; Thio, Y. S.; Bates, F. S. Structure and properties of PBO-PEO diblock copolymer modified epoxy. *Journal of Polymer Science, Part B: Polymer Physics* **2005**, *43*, 1950–1965.
- (33) Garlotta, D. A Literature Review of Poly(Lactic Acid). *Journal of Polymers and the Environment* **2001**, *9*, 63–84.
- (34) Schmidt, S. C.; Hillmyer, M. A. Polylactide Stereocomplex Crystallites as Nucleating Agents for Isotactic Polylactide. *Journal of Polymer Science, Part B: Polymer Physics* **2001**, *39*, 300–313.
- (35) Nofar, M.; Zhu, W.; Park, C. B.; Randall, J. Crystallization kinetics of linear and long-chain-branched polylactide. *Industrial and Engineering Chemistry Research* 2011, 50, 13789–13798.

- (36) Patterson, A. L. The Scherrer Formula for X-Ray Particle Size Determination. *Physical Review* **1939**, *56*, 978–982.
- (37) Wong, Y. S.; Stachurski, Z. H.; Venkatraman, S. S. Orientation and structure development in poly(lactide) under uniaxial deformation. *Acta Materialia* **2008**, *56*, 5083–5090.
- (38) Strobl, G. The physics of polymers: Concepts for understanding their structures and behavior; Springer Berlin Heidelberg, 2007; pp 1–518.
- (39) Alexander, L. E. X-Ray Diffraction Methods in Polymer Science; Robert E. Krieger Publishing Company, 1969.
- (40) Stoclet, G.; Seguela, R.; Lefebvre, J. M.; Elkoun, S.; Vanmansart, C. Strain-induced molecular ordering in polylactide upon uniaxial stretching. *Macromolecules* 2010, 43, 1488–1498.
- (41) Stoclet, G.; Seguela, R.; Vanmansart, C.; Rochas, C.; Lefebvre, J. M. WAXS study of the structural reorganization of semi-crystalline polylactide under tensile drawing. *Polymer* **2012**, *53*, 519–528.
- (42) Yin, Y.; Zhang, X.; Song, Y.; Vos, S. D.; Wang, R.; Joziasse, C. A.; Liu, G.; Wang, D. Effect of nucleating agents on the strain-induced crystallization of poly(l-lactide). *Polymer* **2015**, *65*, 223–232.
- (43) Razavi, M.; Wang, S.-Q. Why is crystalline poly(lactic acid) brittle at room temperature? *Macromolecules* **2019**, *52*, 5429–5441.

# TOC Graphic

